A new class of thermotropic lanthanidomesogens: Eu(III) nitrate complexes with mesogenic 4-pyridone ligands

Electronic supplementary information

Amalia Pană[a], Florentina L. Chiriac[a], Mihai Secu[b], Iuliana Pasuk[b], Marilena Ferbinteanu[a], Marin Micutz[c], Viorel Cîrcu[a]

[a] Department of Inorganic Chemistry, University of Bucharest, 23 Dumbrava Rosie st, sector 2, Bucharest 020464, Romania, e-mail: viorel_carcu@yahoo.com, viorel.circu@chimie.unibuc.ro

[b] National Institute of Materials Physics, P.O. Box MG-7, Magurele, 077125, Romania

[c] Department of Physical Chemistry, University of Bucharest, 4-12 Elisabeta Blvd., Bucharest 030018, Romania

Content:

1. Characterisation methods p. 2
2. Scheme 1. Synthesis of Eu(III) 4-pyridone liquid crystals p. 3
3. Synthesis of 4-pyridone derivatives **2a-c** p. 3
4. Synthesis of Eu(III) complexes **3a-e** p. 4
5. Fig. S1. The TG curves for Eu(III) complexes **3a-e**. p. 5
6. Fig. S2. The TG curves for **2a** and its Eu(III) complex **3a**. p. 6
7. Fig. S3. First (left) and second (right) DSC heating-cooling cycles for **3a**. p. 6
8. Fig. S4. First (left) and second (right) DSC heating-cooling cycles for **3b**. p. 7
9. Fig. S5. First (left) and second (right) DSC heating-cooling cycles for **3c**. p. 7
10. Fig. S6. First (left) and second (right) DSC heating-cooling cycles for **3d**. p. 8
11. Fig. S7. Details of the packing network for **3e** showing the hydrogen bonds and short contacts. The solvent molecules are omitted for clarity. p. 8
12. Fig. S8. The packing along *a* axis for **3e**. The solvent molecules are omitted for clarity. p. 9
13. Fig. S9. The packing along *b* axis for **3e**. The solvent molecules are omitted for clarity. p. 9
14. Fig. S10. The packing along *c* axis for **3e**. The solvent molecules are omitted for clarity. p. 10
15. Table S1. Crystallographic data for **3e.** p. 11
16. Table S2. Selected bond lengths and angles for **3e** p. 12
17. Fig. S11. POM pictures for **3b** at 45°C without (left) and with UV light irradiation (right). p. 12
18. Fig. S12. POM pictures for **3c** at 110°C and 105°C. p. 13
19. Fig. S13. POM picture for **3d** at 104°C. p. 13
20. Fig. S14. POM picture for **2b** at 70°C (left) and for **2c** at 55°C (right). p. 14
21. Table S3. X-ray powder diffraction data for Eu(III) complexes p. 14
22. Fig. S15. XRD powder pattern for **3b** at 50°C. p. 15
23. Fig. S16. XRD powder pattern for **3c** at 50°C. p. 15
24. Fig. S17. XRD pattern for **3d** recorded on cooling from the isotropic state at 70°C (top) and 50°C (bottom). p. 16
25. Table S4. The emission lifetimes of Eu(III) complexes recorded in solid-state p. 17
26. Fig. S18. The emission spectra for Eu(III) complexes **3a-d**. p. 17
27. Fig. S19. Temperature-dependent emission spectra for **3b** on heating the glassy state from 25°C up to 150°C. p. 18

28. Fig. S20. Detection of I-SmA transition for **3b**: intensity of the $^5D_0 \rightarrow {}^7F_2$ transition versus temperature. At the I-SmA transition (94°C) the emission intensity drops significantly. p. 18
29. References p. 18

Characterisation methods. All the chemicals were used as supplied. C, H, N analyses were carried out with a Perkin Elmer instrument. IR spectra were recorded on a Bruker spectrophotometer using KBr pellets. UV-VIS absorption spectra were recorded by using a Jasco V-660 spectrophotometer. ^{1}H and ^{13}C NMR spectra were recorded on a Varian Gemini 300 BB spectrometer operating at 300 MHz, using $CDCl_3$ as solvent. ^{1}H chemical shifts were referenced to the solvent peak position, δ 7.26 ppm. The phase assignments and corresponding transition temperatures for the 4-pyridone ligands and their Eu(III) complexes were determined by polarising optical light microscopy (POM) using a Nikon 50iPol microscope equipped with a Linkam THMS600 hot stage and TMS94 control processor. These observations were made on untreated glass slides. Temperatures and enthalpies of transitions were investigated using differential scanning calorimetry (DSC) with a Diamond DSC Perkin Elmer instrument. The materials were studied at different scanning rates after being encapsulated in aluminium pans. Two or more heating/cooling cycles were performed on each sample with variable scanning rate (2, 5 and 10°C/min). Mesophases were assigned by their optical texture and powder X-ray diffraction data. The powder X-ray diffraction measurements were made on a D8 Advance diffractometer (Bruker AXS GmbH, Germany), in parallel beam setting, with monochromatized Cu–$K_{\alpha 1}$ radiation (λ=1.5406 Å), scintillation detector, and horizontal sample stage. The measurements were performed in symmetric (θ-θ) geometry in the 2θ range from 1.5° to 10° or 30° in steps of 0.02°, with measuring times per step in the 5-40 s range. The temperature control of the samples during measurements was achieved by adapting a home-made heating stage to the sample stage of the diffractometer. Variable temperature emission spectra in solid state were recorded with an OceanOptics QE65PRO spectrometer attached to the microscope and using a Nikon Intensilight excitation source. Photoluminescence (PL) spectra and PL lifetimes measurements have been recorded at room temperature using a Jobin Yvon Fluorolog spectrophotometer; the spectra were not corrected for the spectral sensitivity. Thermogravimetric analysis was performed on a TA Q50 TGA instrument using alumina crucibles and nitrogen as purging gas. The heating rate employed was 10°C min^{-1} from room temperature (approximately 25°C) to 550°C.

Intensity data for a single crystal of **3e** were collected using Mo K_α radiation (λ = 0.71073 Å) on a Rigaku R-Axis Rapid II diffractometer. The data were collected at a temperature of 20±1°C using the ω scan technique to a maximum 2θ value of 55.0°. Omega scans of several intense reflections, made prior to data collection, had an average width at half-height of 0.00° with a take-off angle of 6.0°. The data were corrected for Lorentz and polarization effects. The crystal structure contains two crystallization solvent molecules, one being disordered. The structure was solved by heavy-atom Patterson methods[1] and expanded using Fourier techniques. Refinement of F^2 was done against all reflections. The weighted R factor, wR2, and goodness of fit S are based on F^2. Conventional R factors are based on F, with F set to zero for negative F^2. The structure suffers from considerable disorder. Terminal phenyl rings for two ligands are disordered among two different orientations,

however, in different ways. For C19-C24 the ratio is 55:45 % while for C31-C36 occupancies refined to 50:50%. Adequate constraints were applied to maintain ring shape and distances. While one site of solvent molecule CH_3CN is fully occupied, at a second site three different orientations were derived resulting in occupancies 50:35:15%. Similarity constraints helped to avoid unreasonable deviations in molecular shape. For all hydrogen atoms riding models were applied in final stages of refinement. All calculations were performed using the CrystalStructure[2] crystallographic software package except for refinement, which was performed using SHELXL-2014/7.[3] Crystallographic data have been deposited to the Cambridge Structural Data Base and registered as CCDC 1403398.

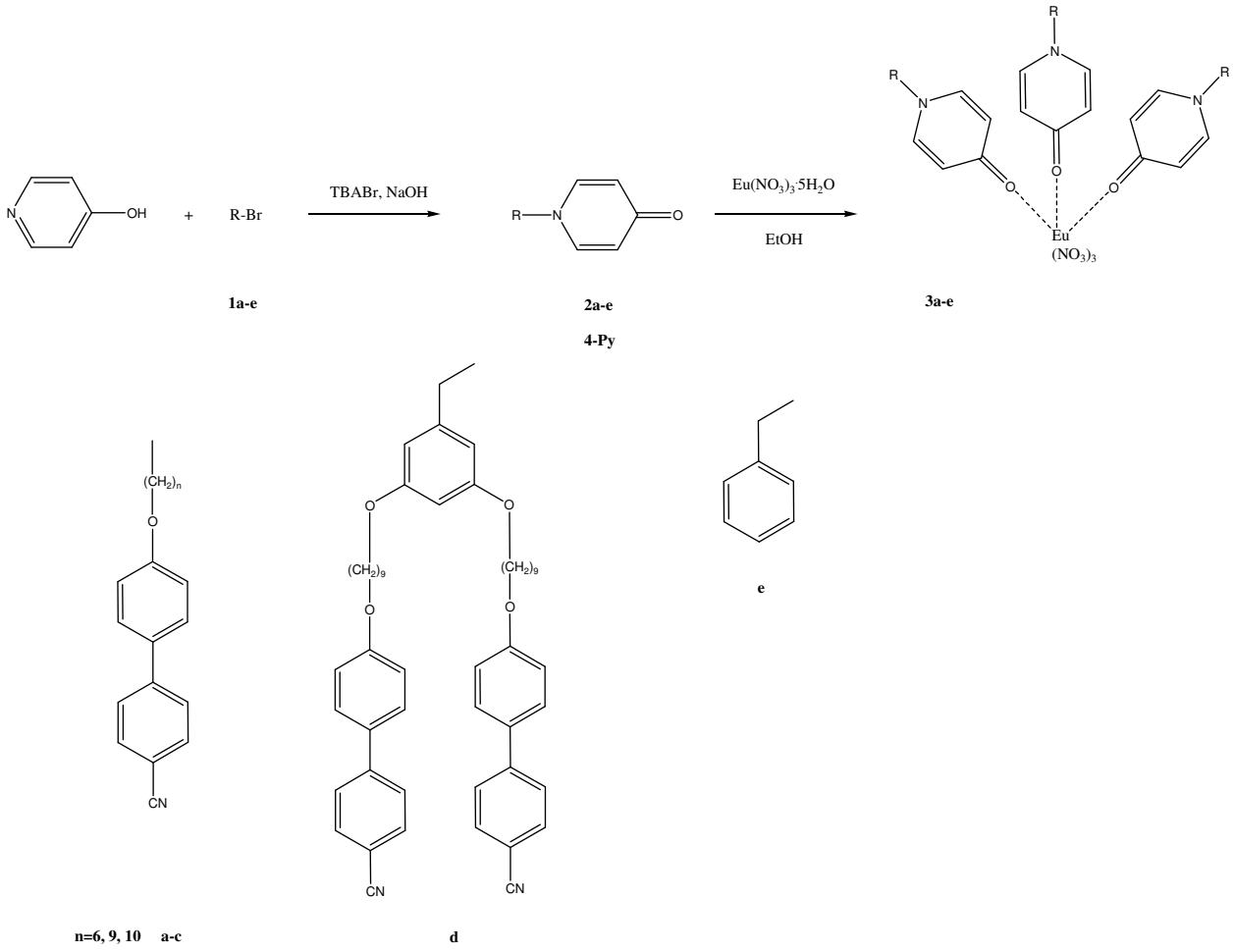

Scheme 1. Synthesis of Eu(III) 4-pyridone liquid crystals

Synthesis of 4-pyridone derivatives 2a-c

To a mixture of 4-hydroxypyridine (4.34g, 10.8mmol) and tetrabutylammonium bromide (0.43g, 1.35mmol) in tetrahydrofuran, was added an aqueous 2N NaOH solution (NaOH equivalent to 4-hydroxypyridine). After this solution became clear, 4'-(n-bromoalkyloxy)-biphenyl-4-carbonitrile was added (4.34g, 10.8mmol) and the mixture was heated to reflux under nitrogen for 2 days. After cooling, the solvent phase was removed by rotary evaporation and the crude product was extracted with a mixture dichloromethane:water (1/1). The organic

layers were collected and dried on anhydrous Na_2SO_4. The dichloromethane phase was reduced and the residue was purified on a silica gel chromatography column using as an eluent a mixture of dichloromethane:methanol (95:5).

2a. White solid. Yield: 51 %. Calcd. For $C_{24}H_{22}N_2O_2$: %C 77.81; %H 5.99; %N 7.56; Found: %C 77.57; %H 6.23; %N 7.47. ^{1}H-RMN ($CDCl_3$, 75MHz): 7.63 (m, 4H), 7.51 (d, 2H, J=8.7Hz), 7.28 (d, 2H, J=8.5Hz), 6.96 (d, 2H, J=8.5Hz), 6.38 (d, 2H, J=8.5Hz), 3.99 (t, 2H, J=6.7Hz), 3.79 (t, 2H, J=6.7Hz), 1.86-1.36 (m, 8H).^{13}C-RMN ($CDCl_3$, 75MHz): 178.7, 159.5, 145.1, 139.7, 132.5, 130.4, 128.3, 127, 119, 118.7, 114.5, 110.0, 67.5, 56.9, 30.8, 28.9, 25.9, 25.6.IR (cm^{-1}): 2938, 2866, 2224, 1639, 1600, 1555, 1493, 1471, 1395, 1289, 1249, 1179, 1032, 995, 846, 821, 740, 657, 557, 529.

2b White solid. Yield: 56 %. Calcd. For $C_{27}H_{28}N_2O_2$: %C 78.61; %H 6.84; %N 6.79; Found: %C 78.47; %H 6.93; %N 6.62. ^{1}H-RMN ($CDCl_3$, 75MHz): 7.64 (m, 4H), 7.51 (d, 2H, J=6.7Hz), 7.27 (d, 2H, J=8.5Hz), 6.97 (d, 2H, J=8.5Hz), 6.38 (d, 2H, J=6.7Hz), 3.98 (t, 2H, J=6.7Hz), 3.75 (t, 2H, J=6.7Hz), 1.76 (m, 4H), 1.48-1.32 (10H). ^{13}C-RMN ($CDCl_3$, 75MHz): 178.7, 159.7, 145.2, 139.6, 132.5, 131.2, 128.3, 127, 119.1, 118.6, 115, 110.0, 68.0, 57.0, 30.8, 29.6, 26.1, 25.9. IR (cm^{-1}): 2928, 2855, 2222, 1638, 1598, 1562, 1495, 1469, 1402, 1379, 1319, 1256, 1044, 853, 827, 725, 661, 555, 531.

2c White solid. Yield 88%. Calcd. For $C_{28}H_{30}N_2O_2$: %C 78.84; %H 7.09; %N 6.57; Found: %C 78.56; %H 7.21; %N 6.38. ^{1}H-NMR ($CDCl_3$, 300 MHz): 7.68 – 7.61 (m, 4H), 7.51 (d, 2H, J=6.7Hz), 6.97 (d, 2H, J=8.7Hz), 6.43 (d, 2H, J=8.7 Hz), 3.99 (t, 2H, J=6.5 Hz), 3.79 (t, 2H, J=7.1Hz), 1.79 – 1.75 (m, 4H), 1.46 – 1.35 (m, 12H). ^{13}C-NMR ($CDCl_3$, 75 MHz): 179.0, 159.8, 145.3, 139.8, 132.6, 131.3, 128.4, 127.1, 119.2, 118.7, 115.4, 110.0, 68.2, 57.2, 31.0, 30.9, 29.4, 29.3, 29.2, 29.1, 29.0, 26.2, 26.1. IR (KBr disc, cm^{-1}): 2923, 2855, 2224, 1638, 1603, 1537, 1494, 1477, 1398, 1291, 1248, 1192, 1178, 1040, 979, 863, 823, 659, 567, 530.

Synthesis of 2d. To a mixture of 4-hydroxypyridine (2.17g, 5.4mmol) and tetrabutylammonium bromide (0.22g, 0.7 mmol) in tetrahydrofuran, an aqueous 2N NaOH solution (NaOH equivalent to 4-hydroxypyridine) was added. To this mixture, bromide derivative prepared by a slightly modified procedure as reported elsewhere[4] (5 g, 5.7 mmol) was added, and the reaction mixture was heated under reflux in nitrogen overnight. Then, the solvent was removed in vacuum and the crude product was extracted with a mixture dichloromethane:water (1/1). The organic layers were collected and dried over anhydrous Na_2SO_4. The dichloromethane phase was reduced and the residue was purified on a silica gel chromatography column using as an eluent a mixture of dichloromethane:methanol (95:5). The solid was recrystallized from a mixture dichloromethane/ether. Yield 75%, white solid. Calcd. For $C_{56}H_{61}N_3O_5$: %C 78.57; %H 7.18; %N 4.91; Found: %C 78.61; %H 7.46; %N 4.63. ^{1}H-NMR ($CDCl_3$, 300 MHz): 7.69 – 7.61 (m, 8H), 7.52 (d, 4H, J=8.3Hz), 7.37 (d, 2H, J=8.5Hz), 6.98 (d, 4H, J=8.4 Hz), 6.54 (d, 2H, J=7.0 Hz), 6.41 (s, 1H), 6.25, 6.26 (s, 2H), 4.85 (s, 2H), 3.99 (t, 4H, J=6.4 Hz), 3.88 (t, 4H, J=6.4 Hz), 1.75 (m, 8H), 1.47 – 1.33 (m, 20H). ^{13}C-NMR ($CDCl_3$, 75 MHz): 178.7, 161.0, 159.7, 145.2, 140.2, 136.6, 132.5, 131.2, 128.3, 127.0, 119.1, 118.7, 115.1, 110.0, 105.8, 101.1, 68.2, 29.5, 29.3, 29.2, 29.1, 26.0. IR (KBr disc, cm^{-1}): 2925, 2853, 2224, 1639, 1602, 1558, 1495, 1469, 1351, 1292, 1251, 1180, 1158, 1053, 850, 822, 660, 562, 531.

2e Yield 55%. ^{1}H-NMR ($CDCl_3$, 300 MHz): 7.38-7.32 (m, 5H), 7.19-7.16 (m, 2H), 6.40 (d, 2H, J=8.5Hz), 4.94 (s, 2H). ^{13}C-NMR ($CDCl_3$, 75 MHz): 178.9, 140.0, 134.7, 129.4, 129.0, 127.3, 118.9, 60.2. IR (KBr disc, cm^{-1}): 1638, 1562, 1501, 1454, 1403, 1378, 1206, 1184, 972, 853, 731, 692, 596, 514, 483.

Synthesis of Eu(III) complexes 3a-e

A solution of $Eu(NO_3)_3{\cdot}5H_2O$ (0.045g, 0.1mmol) in ethanol was added dropwise with continuous stirring to a hot solution of a corresponding 4-pyridone derivative **2a-e** (0.3mmol) in ethanol. A white precipitate was formed immediately. The reaction mixture was stirred at 70^{o}C for two hours. The white precipitate was filtered off, taken in dichloromethane and filtered over Celite to remove any insoluble products. The solvent was removed in vacuo and the solid product was recrystallised from hot ethanol. The white solid was filtered, washed several times with cold ethanol and dried in vacuo.

3a White solid. Yield 30%. Calcd. For $C_{72}H_{72}EuN_9O_{15}$: %C 59.42; %H 4.99; %N 8.66; Found: %C 59.27; %H 5.16; %N 8.46. IR (KBr disc, cm^{-1}): 2937, 2861, 2223, 1636, 1602, 1536, 1493, 1466, 1396, 1309, 1250, 1187, 1031, 858, 820, 659, 564, 532.

3b White solid. Yield 68%. Calcd. For $C_{81}H_{90}EuN_9O_{15}$: %C 61.51; %H 5.74; %N 7.97; Found: %C 61.45; %H 5.85; %N 7.78. IR (KBr disc, cm^{-1}): 2928, 2854, 2224, 1638, 1603, 1537, 1494, 1467, 1385, 1294, 1250, 1184, 1030857, 822, 660, 563, 532.

3c White solid. Yield 45%. Calcd. For $C_{84}H_{96}EuN_9O_{15}$: %C 62.14; %H 5.96; %N 7.76; Found: %C 61.95; %H 6.07; %N 7.57. IR (KBr disc, cm^{-1}): 2927, 2854, 2224, 1638, 1603, 1537, 1493, 1467, 1396, 1310, 1294, 1250, 1182, 998, 855, 821, 659, 563, 533.

3d White solid. Yield 50%. Calcd. For $C_{174}H_{195}EuN_{12}O_{24}$: %C 69.88; %H 6.57; %N 5.62; Found: %C 69.72; %H 6.73; %N 5.43. IR (KBr disc, cm^{-1}): 2925, 2853, 2224, 1637, 1602, 1536, 1494, 1467, 1394, 1349, 1293, 1250, 1178, 1055, 1030, 854, 822, 660, 562, 533.

3e White solid. Yield 40%. Calcd. For $C_{36}H_{33}EuN_6O_{12}$: %C 48.38; %H 3.72; %N 9.40; Found: %C 48.19; %H 3.85; %N 9.27. IR (KBr disc, cm^{-1}): 1633, 1558, 1527, 1452, 1393, 1373, 1303, 1198, 1169, 966, 816, 738, 699, 604, 474.

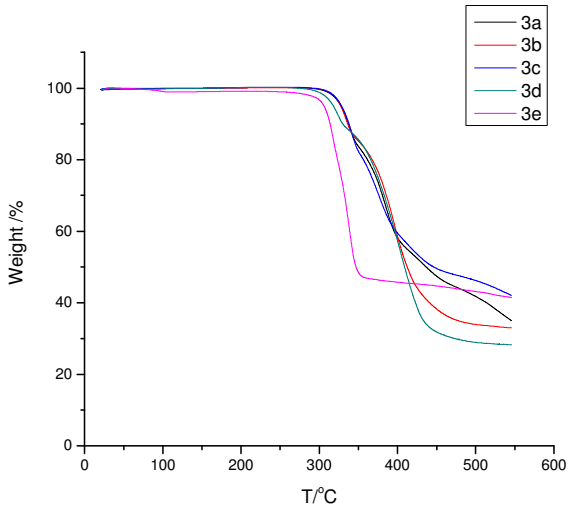

Fig. S1. The TG curves for Eu(III) complexes **3a-e**.

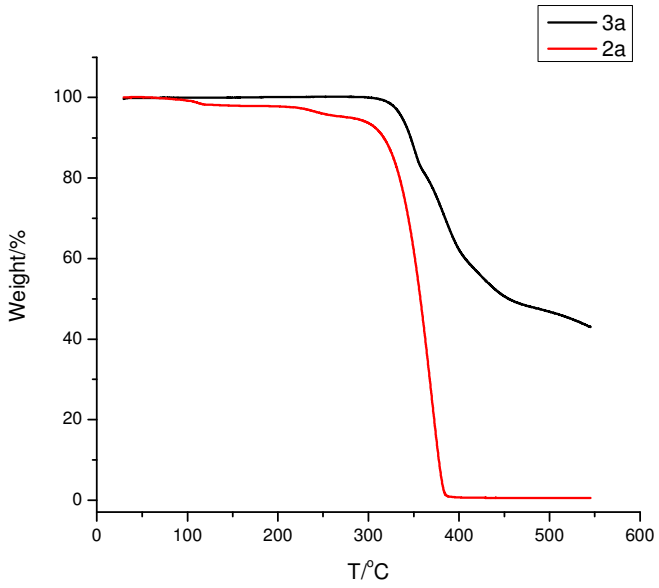

Fig. S2. The TG curves for 4-pyridone ligand **2a** and its Eu(III) complex **3a**.

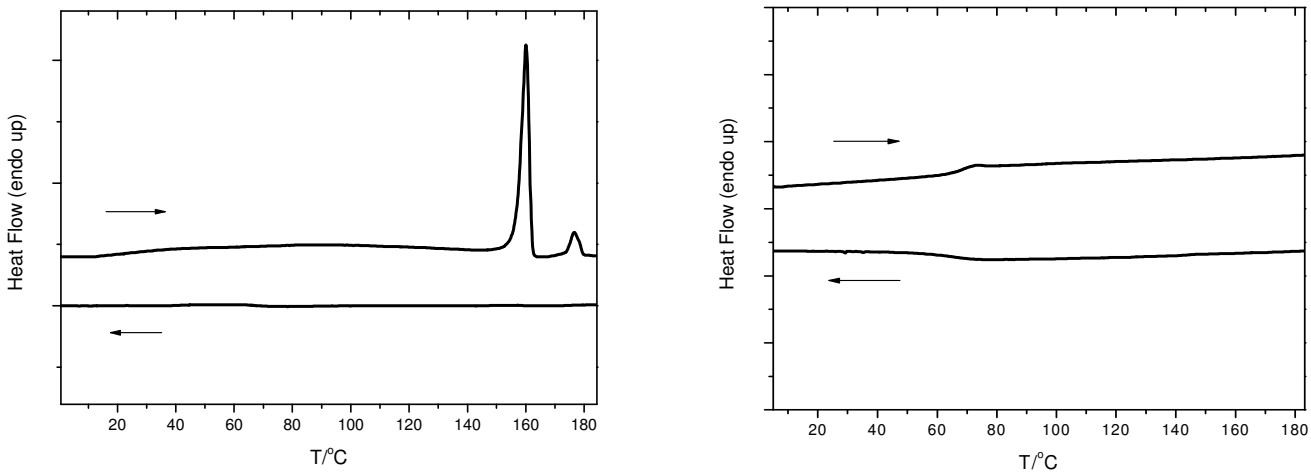

Fig. S3. First (left) and second (right) DSC heating-cooling cycles for **3a**.

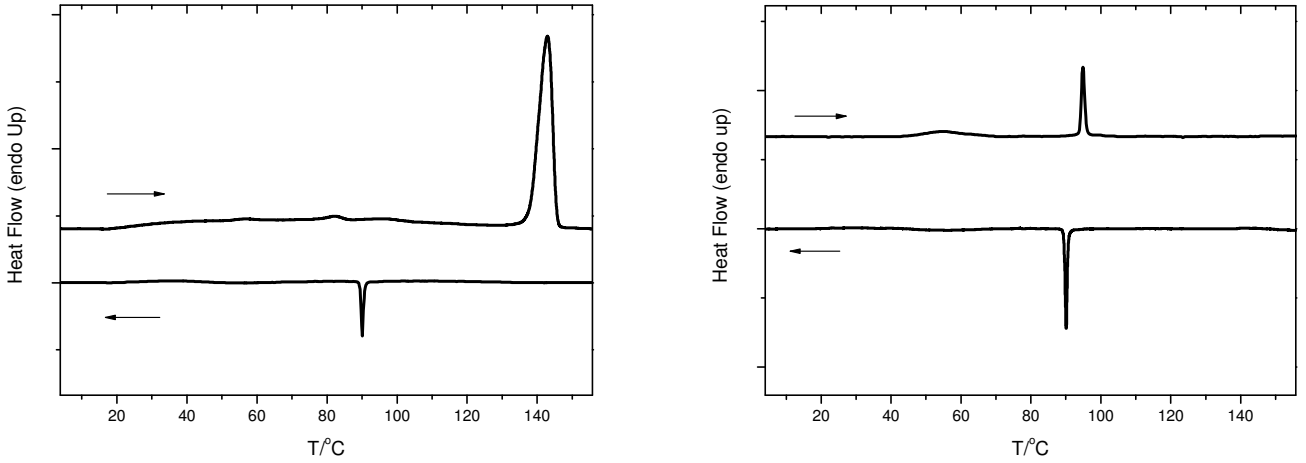

Fig. S4. First (left) and second (right) DSC heating-cooling cycles for **3b**.

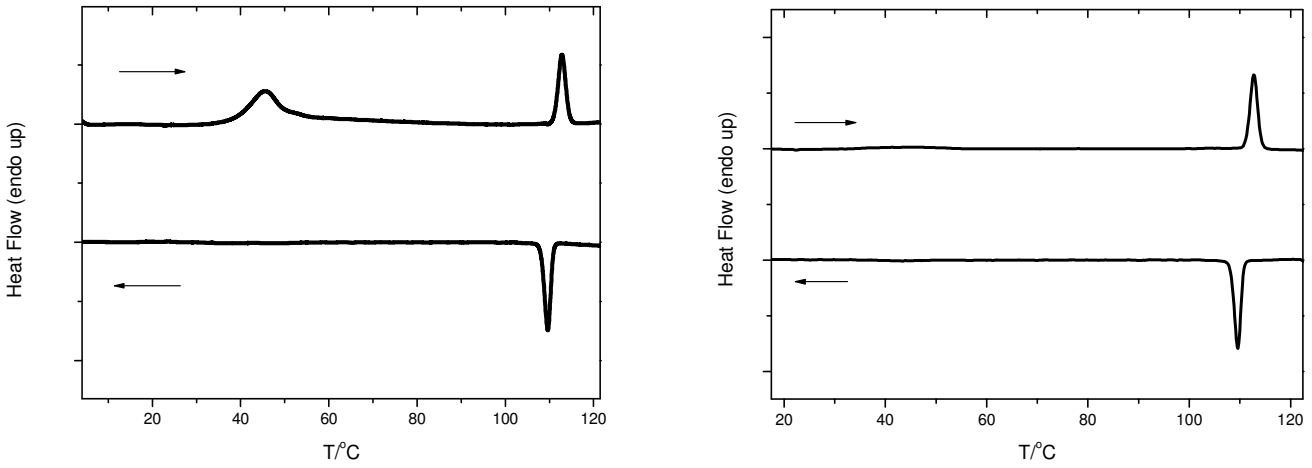

Fig. S5. First (left) and second (right) DSC heating-cooling cycles for **3c**.

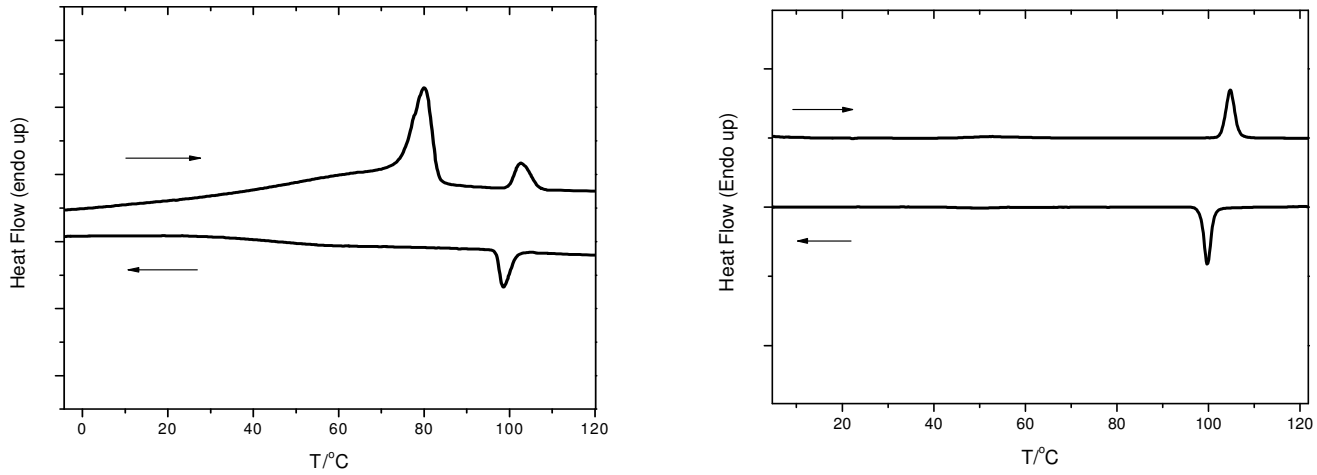

Fig. S6. First (left) and second (right) DSC heating-cooling cycles for **3d**.

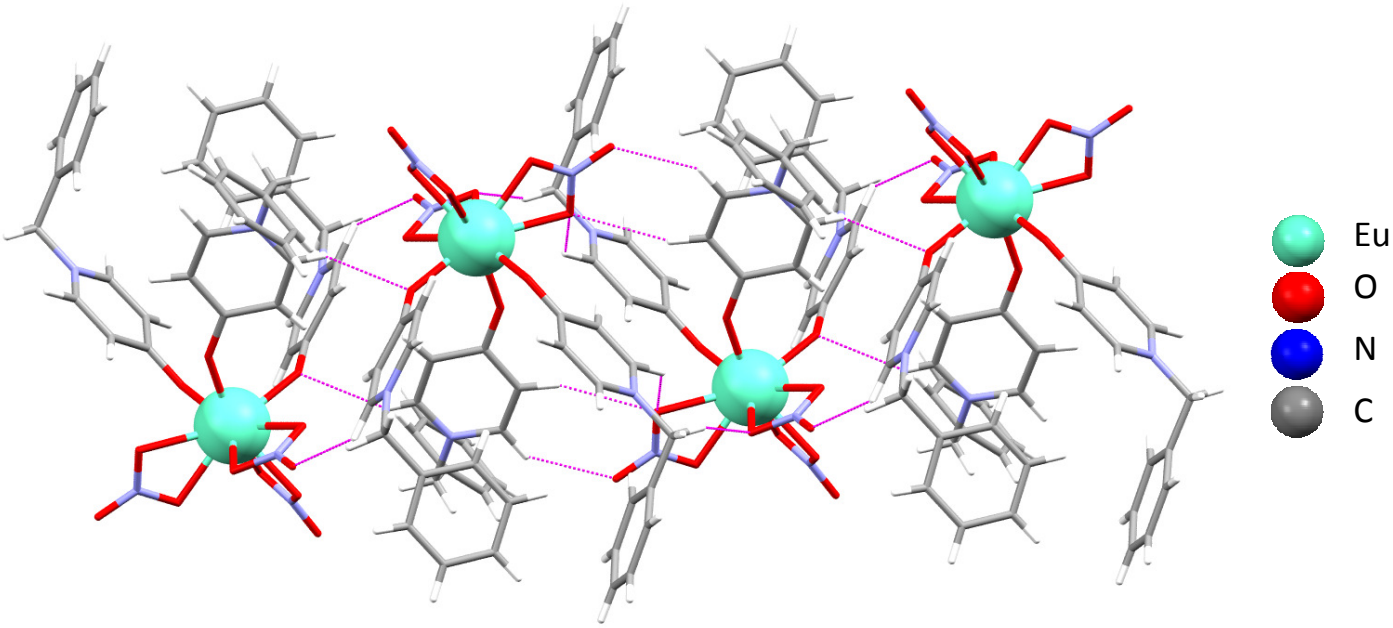

Fig. S7. Details of the packing network for **3e** showing the hydrogen bonds and short contacts. The solvent molecules are omitted for clarity.

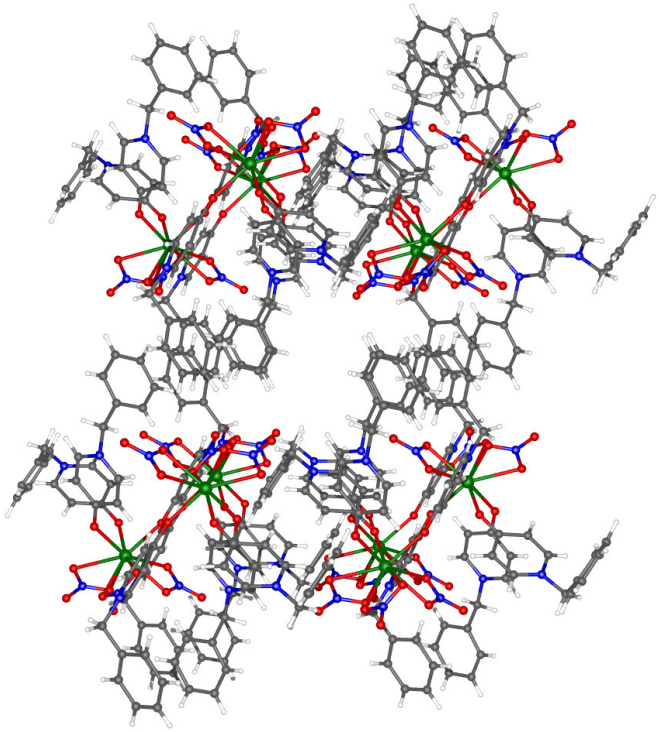

Fig. S8. The packing along *a* axis for **3e**. The solvent molecules are omitted for clarity.

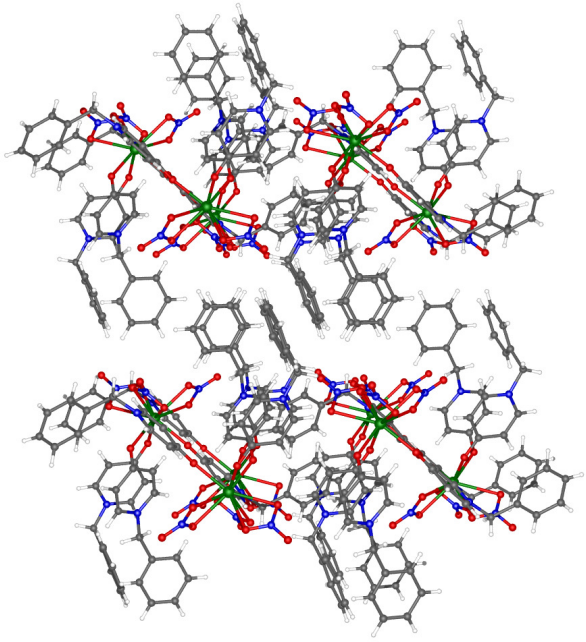

Fig. S9. The packing along *b* axis for **3e**. The solvent molecules are omitted for clarity.

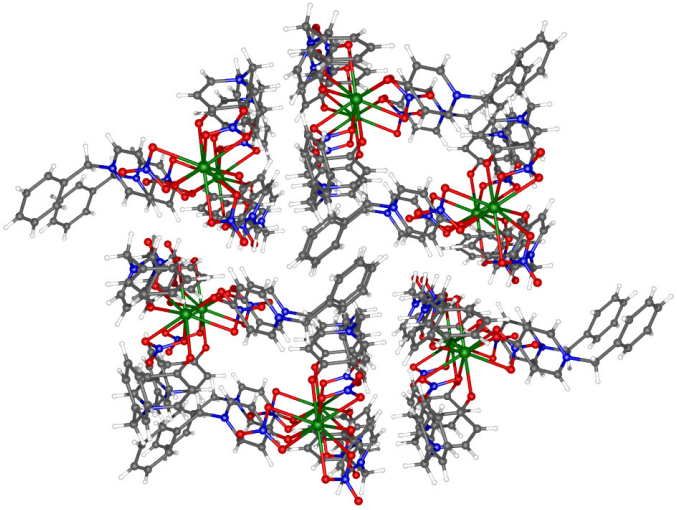

Fig. S10. The packing along *c* axis for **3e**. The solvent molecules are omitted for clarity.

Table S1. Crystallographic data for **3e.**

	3e·2CH$_3$CN
Empirical formula	C40H39EuN8O12
M	975.75
T/K	293(2)
λ/nm	0.71073 Å
Crystal system	triclinic
Space group	*P-1*(#2)
a/ Å	13.2723(4)
b/ Å	13.4162(3)
c/ Å	14.6520(10)
α/°	78.952(6)
β/°	80.569(6)
γ/°	61.141(4)
V/ Å^3	2234.9(2)
Z	2
Calculated density (g.cm^{-3})	1.450
Absorption coefficient μ/mm^{-1}	1.470
F(000)	988
Crystal size/mm	0.30 x 0.20 x 0.15
Crystal color	colourless
θ range for data collection/ °	3 to 27.485
ω range for data collection (χ=45.0, ϕ=270.0)/ °	20 to 200
ω range for data collection (χ=45.0, ϕ=90.0)/ °	20 to 200
h_min, h_max	-17, 17
k_min, k_max	-17, 17
l_min, l_max	-19, 19
Reflections collected / unique	23923 / 9808
Completeness to θ_{max}	0.955
Data / parameters	9808 / 661
Goodness-of-fit	1.058
Final R indices [I>2σ]	*R*1 = 0.0375
R indices (all data)	*R*1 = 0.0308
	w*R*2 = 0.0738

Table S2. Selected bond lengths and angles for **3e**

Eu-O (4-pyridone)	2.318(3); 2.298(2); 2.305(3)
Eu-O (NO_3)	2.488(3); 2.579(3); 2.504(2);
	2.604(3); 2.483(3); 2.590(2)

The shortest distance found for Eu …Eu is 8.57Å.

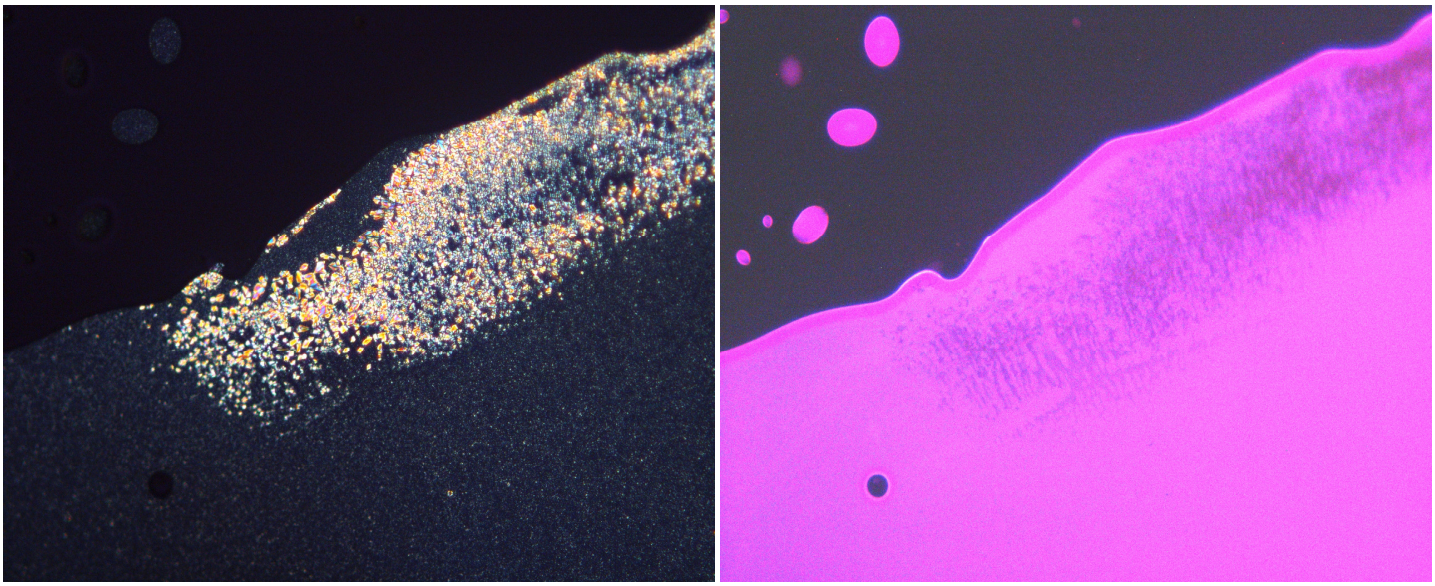

Fig. S11. POM pictures for **3b** at 45^{o}C without (left) and with UV light irradiation (right).

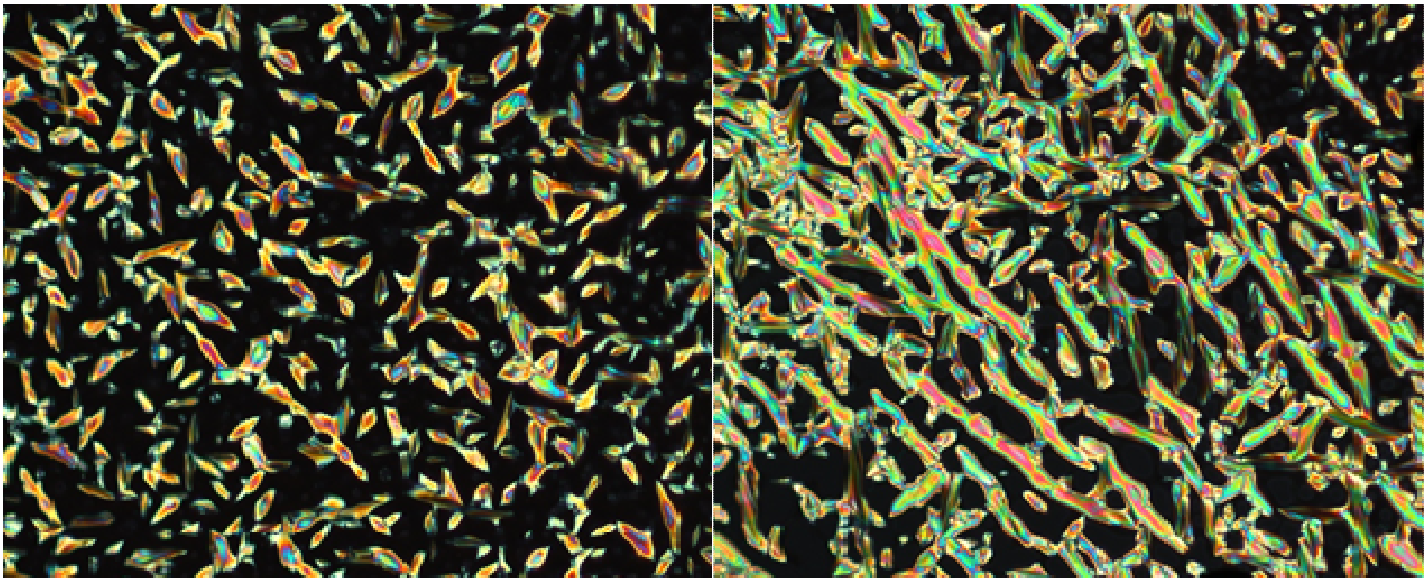

Fig. S12. POM pictures for **3c** at 110°C (left) and 105°C (right).

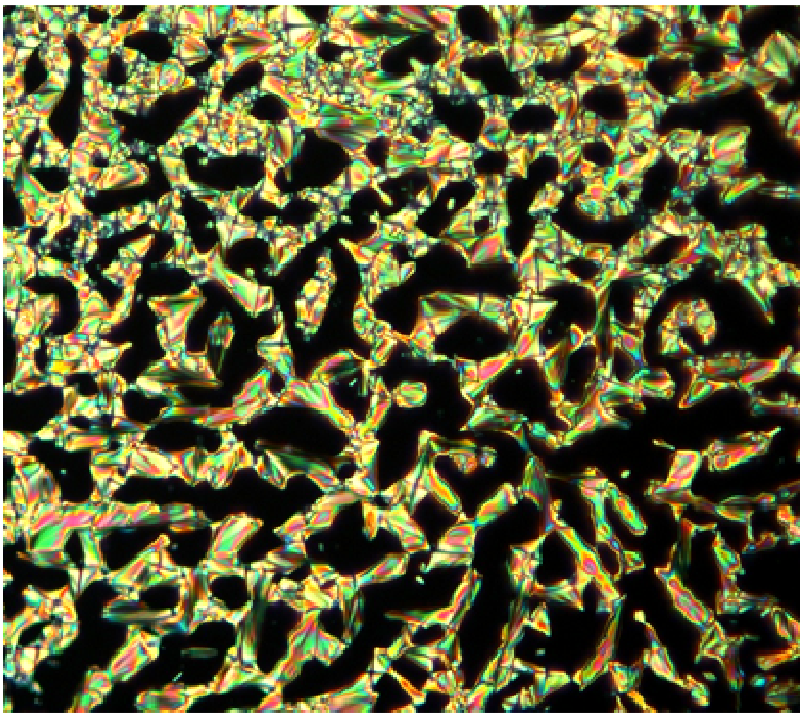

Fig. S13. POM picture for **3d** at 104°C.

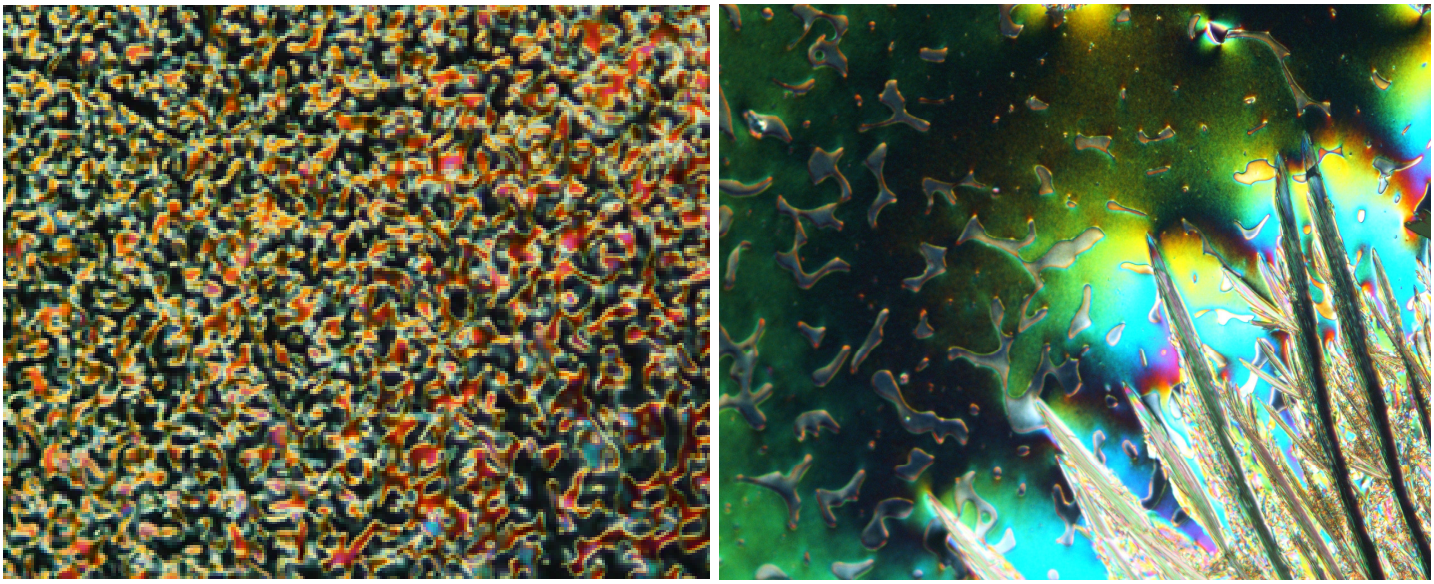

Fig. S14. POM picture for **2b** at 70°C (left) and for **2c** at 55°C (right).

Table. S3. X-ray powder diffraction data for Eu(III) complexes

Compound	T/°C	Phase	2θ/°	d/Å	Indexation
3b	90	SmA	2.54	34.75	d_{001}
			5.16	17.11	d_{002}
			10.66	8.29	
			20.28	4.38	h_{ch}
	50	SmA	2.42	36.47	d_{001}
			5.00	17.66	d_{002}
			10.40	8.50	
			20.66	4.30	h_{ch}
3c	70	SmA	2.38	37.09	d_{001}
			4.68	18.87	d_{002}
			10.93	8.09	
			21.00	4.23	h_{ch}
	50	SmA	2.36	37.41	d_{001}
			4.66	18.95	d_{002}
			11.12	7.95	
			21.06	4.22	h_{ch}
3d	70	SmA	2.04	43.27	d_{001}
			4.10	21.53	d_{002}
			11.67	7.58	
			21.61	4.11	h_{ch}
	50	SmA	2.04	43.27	d_{001}

4.14	21.33	d_{002}
11.98	7.38	
21.50	4.13	h_{ch}

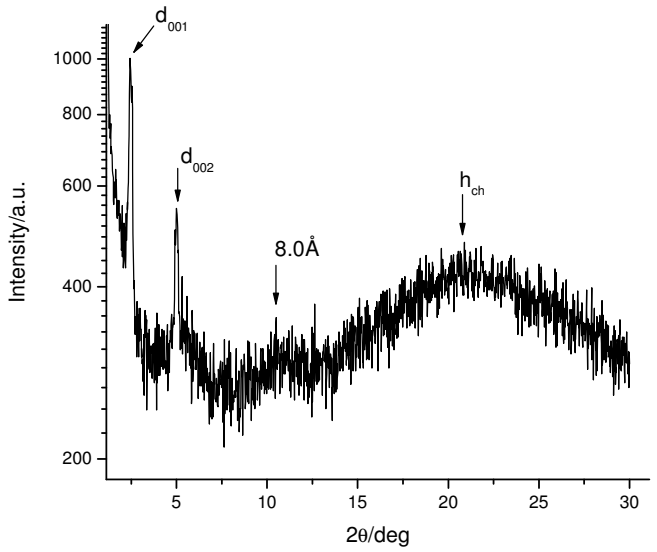

Fig. S15. XRD powder pattern for **3b** at 50°C.

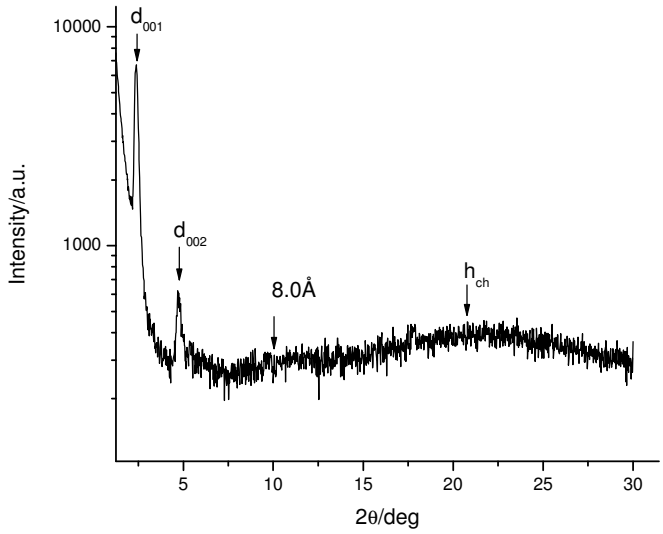

Fig. S16. XRD powder pattern for **3c** at 50°C.

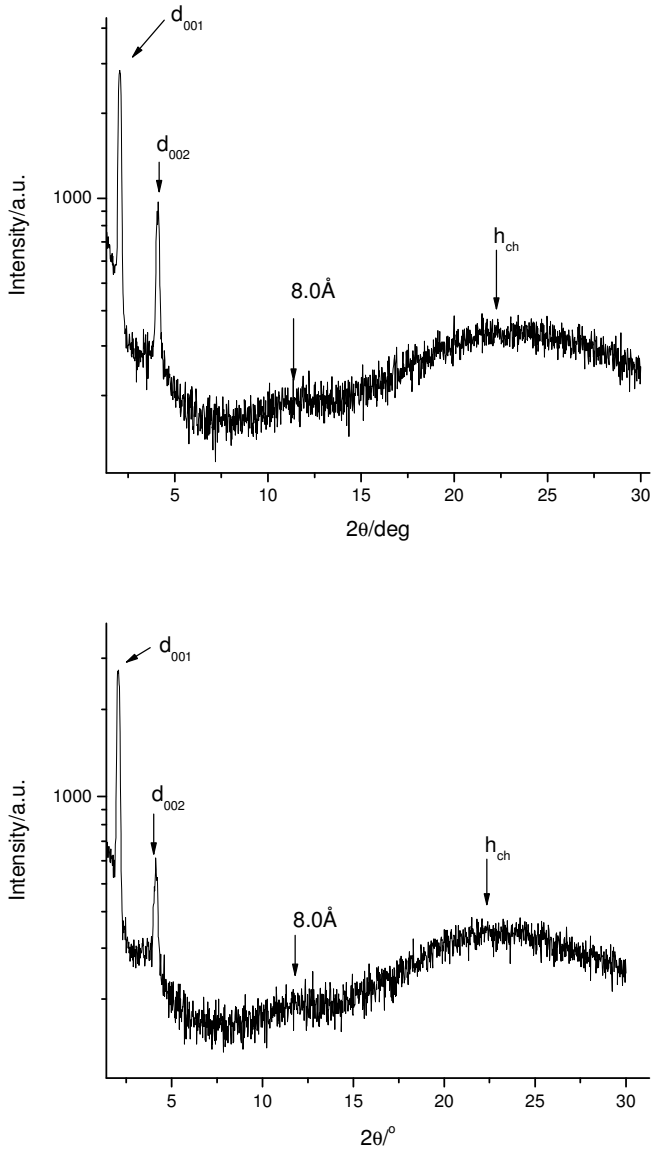

Fig. S17. XRD pattern for **3d** recorded on cooling from the isotropic state at 70^{o}C (top) and 50^{o}C (bottom).

Table S4. The emission lifetimes of Eu(III) complexes recorded in solid-state

Compound	τ/ms[a]
3a	0.72
3b	0.81
3c	0.68
3d	0.58
3e	0.68

[a]The estimated error on the τ values is ±0.01 ms

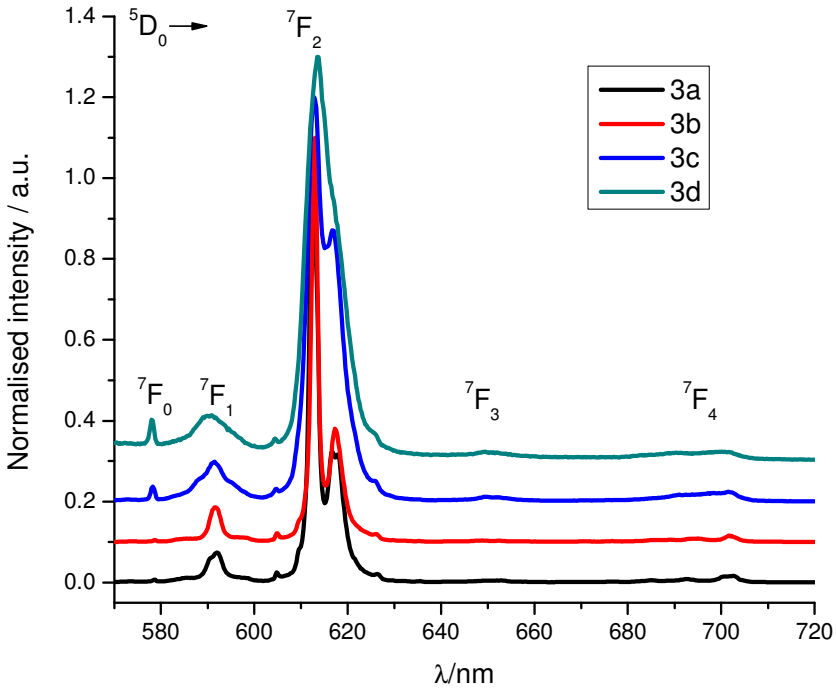

Fig. S18. The emission spectra for Eu(III) complexes **3a-d**.

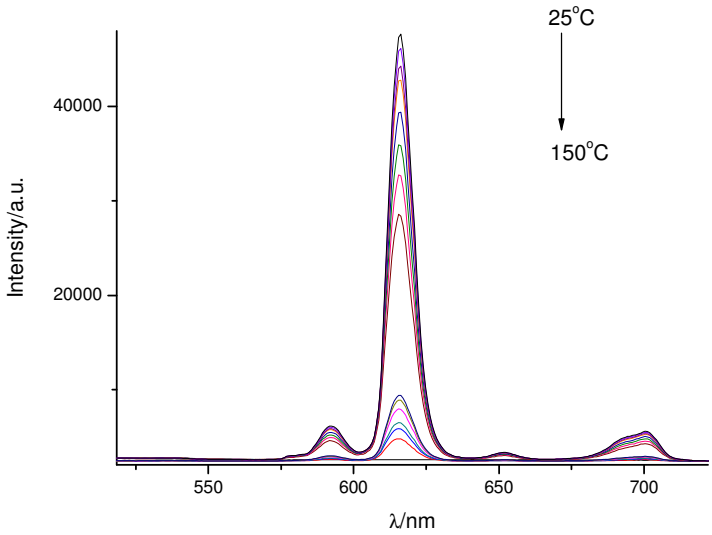

Fig. S19. Temperature-dependent emission spectra for **3b** on heating the glassy state from 25°C up to 150°C.

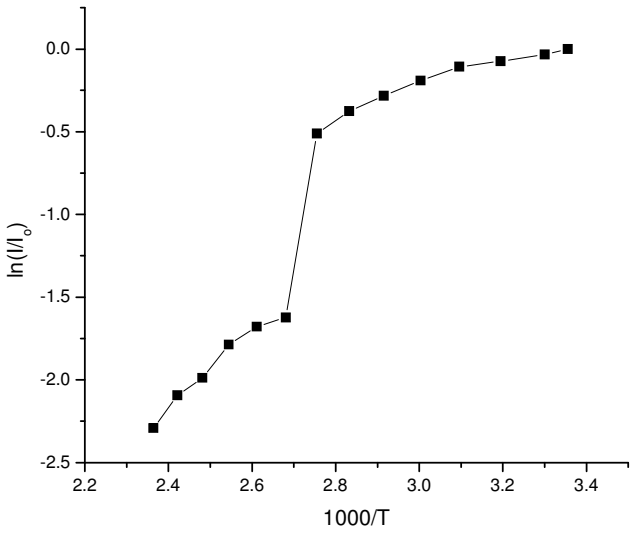

Fig. S20. Detection of I-SmA transition for **3b**: intensity of the $^5D_0 \rightarrow {}^7F_2$ transition versus temperature. At the I-SmA transition (94°C) the emission intensity drops significantly.

References:

1. P.T. Beurskens, G. Admiraal, H. Behm, G. Beurskens, J.M.M. Smits, C. Smykalla, *Z. f. Kristallogr.* 1991, Suppl.4, 99.
2. CrystalStructure 4.0: Crystal Structure Analysis Package, Rigaku Corporation (2000-2010). Tokyo 196-8666, Japan.

3. Sheldrick, G. M. SHELXTL Version 2014/7. http://shelx.uni-ac.gwdg.de/SHELX/index.php.
4. A. Demortiere, S. Buathong, B.P. Pichon, P. Panissod, D. Guillon, S. Begin-Colin, B. Donnio, *Small*, 2010, **6**, 1341-1346.